Izvestiya, Physics of the Solid Earth, Vol. 40, No. 2, 2004, pp. 163–175. Translated from Fizika Zemli, No. 2, 2004, pp. 82–96.

Multidimensional Wavelet Analysis of Time Series of Electrotelluric Observations in Kamchatka

A. A. Lyubushin, Jr.* and G. N. Kopylova**

**Schmidt United Institute of Physics of the Earth, Russian Academy of Sciences, Bol'shaya Gruzinskaya ul. 10, Moscow, 123995 Russia*

***Kamchatka Experimental Seismological Expedition (KESE), Geological Service, Russian Academy of Sciences, Petropavlovsk-Kamchatski, Russia*

Received July 25, 2002

Abstract—The paper presents results of joint multidimensional wavelet analysis of three series of variations in the electrotelluric potential observed at the Verkhnyaya Paratunka station in the Kamchatka Peninsula from October 1, 1996, to June 23, 2001. The analysis was made in order to identify common components in the signals analyzed and compare them with the seismic regime and variations in meteorological parameters. The analysis was based on the method of robust wavelet-aggregated signals, developed by one of the authors for monitoring problems. The average prognostic efficiency of the inferred anomalies is estimated. The analysis revealed the effect of frequency migration of the collectiveness measure peak in the behavior of the study series toward higher frequencies; this effect took place throughout the observation interval. Recently, specific features of this type in the behavior of geophysical characteristics have more often been regarded as a basically new class of strong earthquake precursors.

INTRODUCTION

Modern ideas of seismotectonic (in a more general sense, geodynamic) processes in the crust associated with the nucleation of earthquakes or volcanic eruptions suggest that these processes are observable in natural electromagnetic field variations at the Earth's surface. From the physical standpoint, the electromagnetic monitoring of geodynamic processes is validated, first, by variations in electrical properties of the geological medium (resistivity, conductivity, and polarization) due to tectonic processes and, second, by the mechanoelectrical conversion of the energy of tectonic processes and the excitation of related electromagnetic fields [*Electromagnetic* …, 1982; Gokhberg *et al.*, 1988; Sobolev, 1993; Svetov *et al.*, 1997].

The electrotelluric field (ETF) has been recorded over a few decades in various seismically active regions (including Kamchatka) for the detection of earthquake precursors [Sobolev, 1993; Moroz *et al.*, 1995; Balesta *et al.*, 1999; Uyeda, 1996]. However, notwithstanding numerous communications of observations of diverse ETF variations associated with earthquakes, no clear ideas of the mechanism underlying the formation of such signals have been developed as yet. This is primarily due to the difficulty of interpreting ETF time series affected by diverse and concurrent effects of various external and internal factors. Diverse ETF variations arising due to ionospheric, meteorological, anthropogenic, and other effects prior to any earthquake significantly complicate the identification of signals related to the development of recent geodynamic processes and the nucleation of strong earthquakes.

ETF variation anomalies due to seismotectonic processes can be identified with the use of data processing techniques by which desired signals hidden in strong noise are diagnosed formally, on the basis of their general statistical properties. In this work, data are processed by a robust method of the multidimensional analysis applied to wavelet expansion coefficients of initial time series. The algorithm used here is a modification of the method of aggregated signals [Lyubushin, 1998, 1999, 2000, 2001, 2002].

An aggregated signal is constructed in two stages. First, the initial multivariate series is replaced by a likewise multivariate series of the so-called canonical components, which retain common signals and do not contain local signals. At the second stage, the common signals are additionally enhanced by constructing a single scalar series, their principal component; it is this scalar series that is called the aggregated signal of the initial multivariate time series. These operations can be performed in either the space of Fourier coefficients or the space of wavelet expansion coefficients of the initial data. Each aggregation stage is implemented as a sequence of projections of multidimensional Fourier (wavelet) transforms onto eigenvectors of various spectral (covariance) matrices. All stages of this computational technology are described in detail in [Lyubushin, 1998, 1999, 2000, 2001, 2002]. The use of orthogonal wavelets [Daubechies, 1992; Mallat, 1998] enables the analysis of strongly nonstationary and non-Gaussian series (Fourier methods, albeit formally possible, are ineffective in this case). This paper uses a robust modification of the method of wavelet-aggregated signals

that is stable with respect to high-amplitude outliers in the values of wavelet coefficients [Lyubushin, 2002]. The presence of outliers is due to the ability of wavelet expansions to accumulate maximum information in a relatively small number of coefficients.

DATA OF OBSERVATIONS

Electrotelluric observations aimed at the discovery of earthquake precursors have been conducted in Kamchatka since the 1960s. A description of the observation technique and the results obtained from the 1960s through the first half of the 1990s are given in [Sobolev and Morozov, 1974; Sobolev, 1993; Moroz *et al.*, 1995].

Since 1996, the KESE has conducted continuous recording of the ETF at the Verkhnyaya Paratunka (VP) station (Fig. 1) using a geophysical radiotelemetering system [Moroz *et al.*, 1995; Balesta *et al.*, 1999]. The VP station (52.83° N, 158.12° E) is located in the southern valley of the Paratunka River, near its confluence with the Karymshin River. Structurally, the observation area is located at the intersection of the N–S trending Paratunka graben and the NE trending Karymshin graben. The grabens formed in the Middle Proterozoic, at the time of the last activation of orogenic neotectonic movements in Kamchatka, as a result of subsidence of rock blocks accommodating the rapid uplift of surrounding ridges [*Kamchatka* …, 1974]. In the southern part of the Paratunka graben, these processes continue presently and give rise to the periodic occurrence of swarms of weak tectonic earthquakes.

The area is composed of (in downward order) loose deposits of Quaternary age, a Lower Pleistocene sequence of tuffaceous conglomerates and siltstones, and volcaniclastic rocks of Paleogene–Neogene age. The geological structure of the area is complicated by the emplacement of dacitic intrusive and liparitic extrusive rocks of Neogene age. The area is located within the Karymshin sector of the Paratunka geothermal system [Manukhin and Vorozheikina, 1986]. The VP station is 30 km northeast of the Gorelyi Volcano and 45 km north of the Mutnovskii Volcano [*Active Volcanoes* …, 1991]. The volcanism of the observation period manifested itself mostly in fumarolic activity and rare weak volcano-tectonic earthquakes.

The VP station is a system of three measuring lines, each 70–100 m long, oriented in the N–S (line 1), E–W (line 3), and SW–NE (line 4) directions. The lines are grounded via lead electrodes embedded in pits to a depth of about 2 m. The difference of telluric potentials was recorded at a rate of 1 min with an accuracy of 0.5 mV. The overall duration of observations amounted to four years and eight months (from October 1, 1996, to June 23, 2001).

Previous studies that analyzed results of electrotelluric observations in Kamchatka and other regions revealed a broad spectrum of anomalous signals preceding earthquakes and ranging in amplitude from a few to a few hundreds of mV/100 m units and in length from a few minutes to a few tens of days. Smooth baylike variations and pulsed signals were identified [Sobolev, 1993; Moroz *et al.*, 1995; Uyeda, 1996; and others]. However, Kopylova *et al.* [2001] noted that the majority of diverse variations in Kamchatka can be naturally and adequately accounted for by the effects of external ionospheric sources and seasonal, mostly hydrological and hydrometeorological, factors. The low-frequency ETF variations include seasonal yearly variations with amplitudes from tens to a few hundreds of mV/100 m units and asymmetric baylike variations with amplitudes from a few to a few tens of mV/100 m units due to precipitation in summer and winter thaws (their length is from a few to more than ten days). The highest amplitudes of ETF variations are observed from April through June, when the snow thaws, and in October and November, when considerable autumn precipitation falls (Fig. 2).

The ETF variations with periods of a few minutes to a few tens of hours mainly represent magnetotelluric variations. They include periodic variations with characteristic periods of 12 and 24 h and aperiodic variations of geomagnetic disturbances. The amplitudes of such ETF variations range from a few to a few tens of mV/100 m units.

Figure 2 presents time series of telluric potential differences recorded with the measuring lines described above; the series were obtained by averaging data and their thinning for the transition to a 1-day discretization interval. The plots of the observed electrotelluric data are compared to variations in the average daily air temperature and daily total precipitation derived from observations at the Pionerskaya meteorological station (Kamchatka Department of Hydrometeorology and Environmental Monitoring) 20 km from the VP station. The sensitivity of telluric potential variations to the direction of an individual line is evidence for a strong inhomogeneity of the ETF in the area of the VP station, which agrees with the ideas of mosaic propagation of background ETF variations even within small areas [Deshcherevsky and Sidorin, 2000].

Due to the choice of a 1-day discretization interval, strong high-frequency noise, mainly produced by external factors, was removed from the data. Moreover, the 1-day interval enables a more detailed examination of the low-frequency region of the ETF spectrum, in which the field components due to mechanoelectrical conversions are supposed to linearly depend on the mechanical deformations producing these fields [Svetov *et al.*, 1997]. We also should emphasize that the strongly non-Gaussian and nonstationary behavior of the initial data raises doubts about the validity of their analysis using Fourier expansions. Wavelets provide the most suitable tool for the analysis of precisely this type of data.

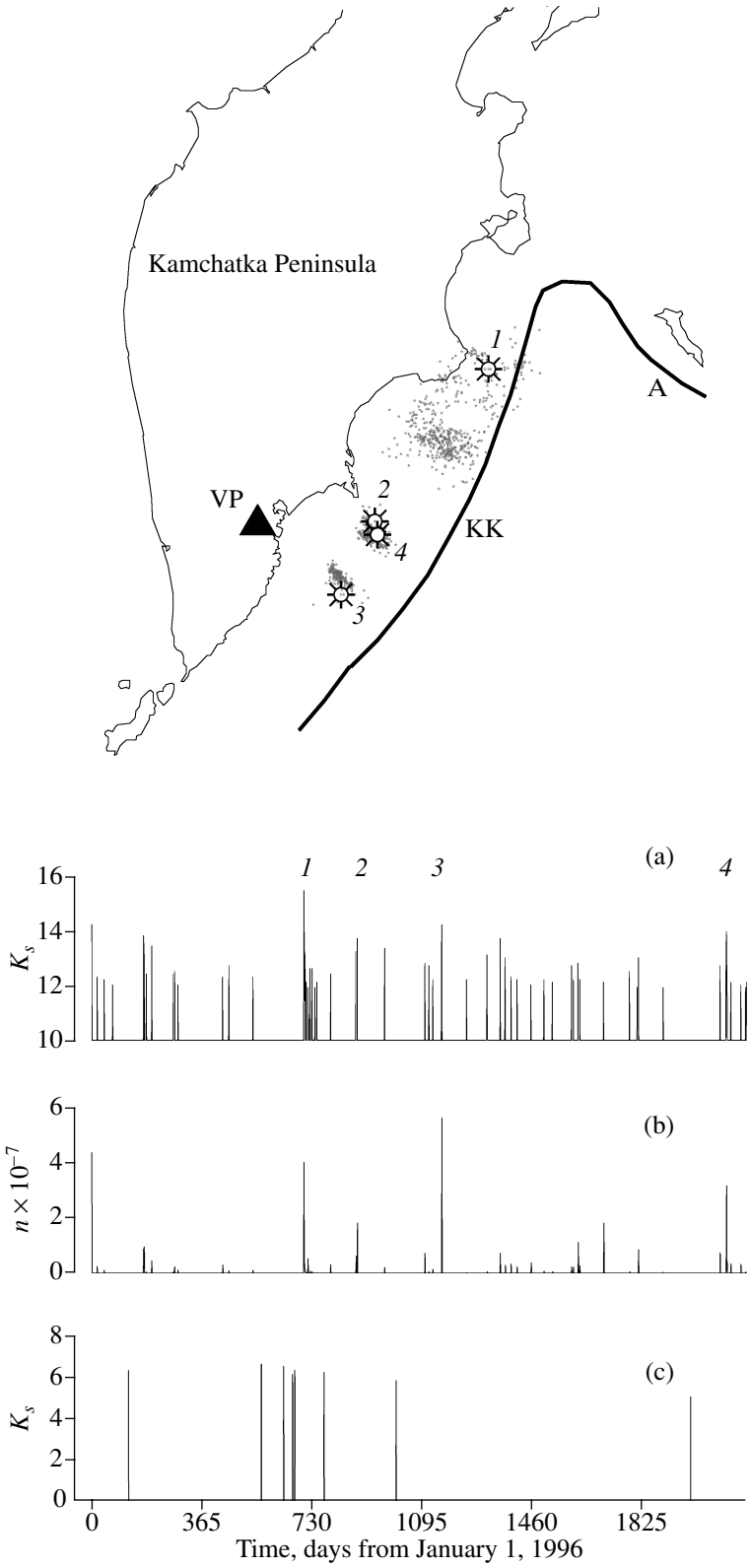

Fig. 1. Schematic map showing the position of the Verkhnyaya Paratunka (VP) station of electrotelluric observations and epicenters of strong earthquakes and their aftershocks: (*1*) December 5, 1997, $M_s = 7.9$; (*2*) June 1, 1998, $M_s = 6.3$; (*3*) March 8, 1999, $M_s = 6.9$; (*4*) October 8, 2002, $M_s = 6.6$; KK, Kurile-Kamchatka deep-sea trench; A, Aleutian deep-sea trench. (a) Earthquakes of 1996–2001 with $K_s \geq 12$, $H \leq 100$ km, and $R \leq 360$ km from the VP station. (b) Day-summarized strain in the VP station area (after Dobrovolskii [1991]). (c) Local weak earthquakes in the VP station area. The broken horizontal line shows the period of electrotelluric observations.

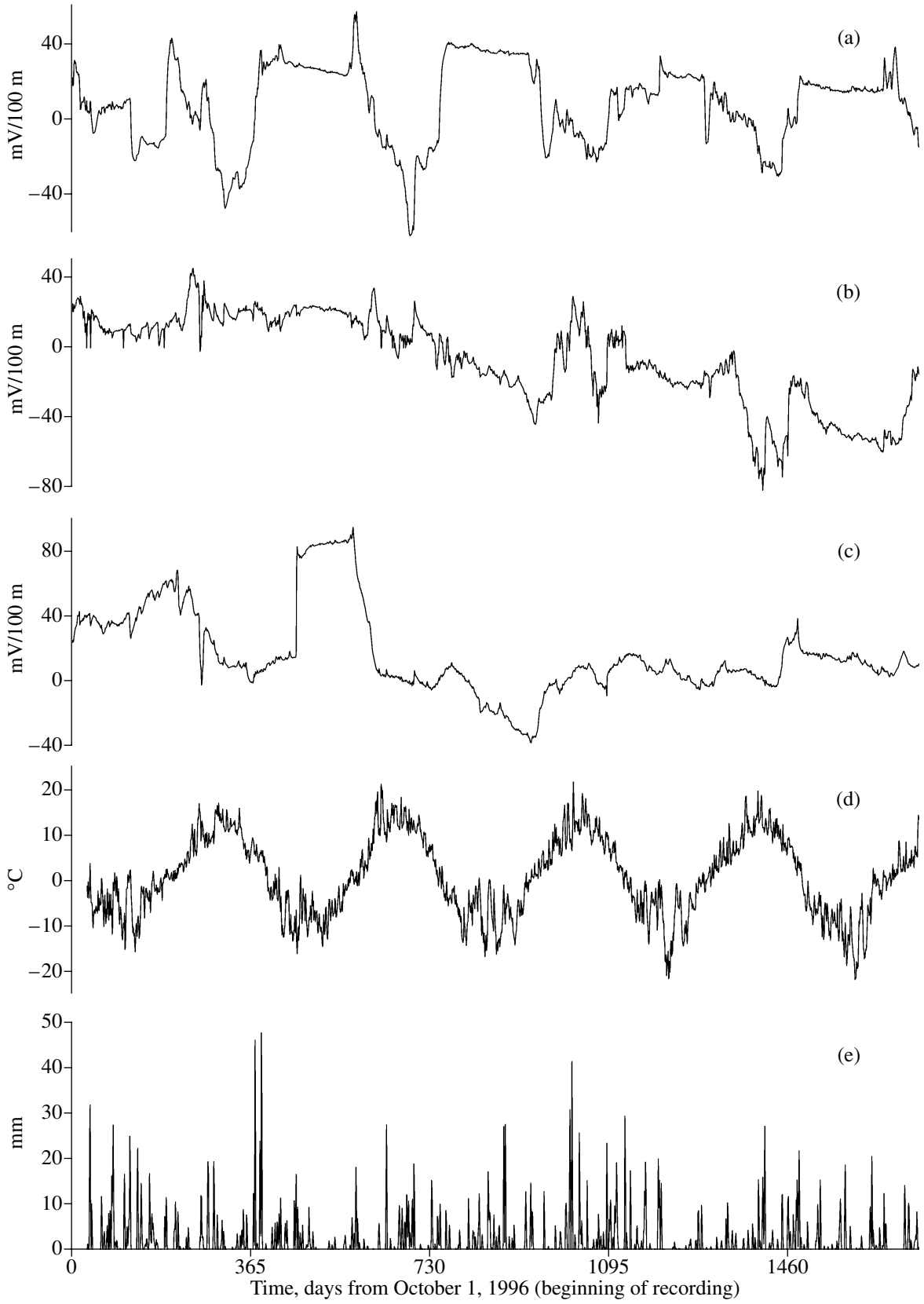

Fig. 2. Initial data after averaging and thinning by 24 times (transition to a 1-day discretization interval) in comparison with hydrometeorological factors: (a–c) measuring lines (a) 1, (b) 3, and (c) 4; (d) daily average air temperature; (e) daily precipitations.

Main characteristics of strong earthquakes of 1996–2001 within 360 km from the Verkhnyaya Paratunka station ($H \le 100$ km)

No. (Fig. 1)	Date	Coordinates, deg		Depth, km	M_s	K_s^{F68}	R*, km	MSK-64 intensity	ε, 10^{-7}
		N	E						
	Jan. 1, 1996	53.90	159.43	0	7.0	14.3	147	3–4	4.2
	June 21, 1996	51.27	159.63	1	7.0	13.9	202	4–5	0.9
1	Dec. 5, 1997	54.64	162.55	10	7.9	15.5	354	5	1.8
	May 28, 1998	51.83	160.25	40	6.0	13.3	187	4	0.5
2	June 1, 1998	52.81	160.37	31	6.3	13.8	151	4–5	1.8
3	Mar. 8, 1999	51.93	159.72	7	6.9	14.3	148	4–5	4.1
	June 3, 2000	52.00	159.10	59	4.9	12.9	114	3–4	1.1
	Aug. 27, 2000	52.68	159.10	87	4.8	12.2	110	3–4	1.8
	Dec. 20, 2000	53.34	159.99	68	5.6	13.1	152	3–4	0.9
4	Oct. 8, 2001	52.65	160.42	28	6.6	13.9	156	4–5	2.0

Note: R is the epicentral distance from the VP station, the MSK-64 intensity is given for the area of Petropavlovsk-Kamchatski, and ε is the strain estimate calculated for the VP station area at the earthquake nucleation stage [Dobrovolskii, 1991].

SEISMICITY

The seismic setting in Kamchatka in the period from 1996 through 2001 reduced mainly to the occurrence of strong earthquakes with magnitudes of 6.3 to 7.9 (Fig. 1; table). In 1996 (before electrotelluric observations), two strong earthquakes, both having the magnitude M = 7.0, occurred on January 1 and June 26 (Fig. 1a).

Strong earthquakes ($M \ge 6.0$) of the observation period. The Kronotski earthquake of December 5, 1997 (M = 7.9; no. 1 in the table and Fig. 1) occurred at a distance of 350 km from the VP station and was followed by numerous aftershocks over a vast (200 × 100 km) area in the Kamchatka and Kronotski bays. This is the strongest event in Kamchatka since 1971. An unusual outburst of seismic activity was observed in December 1997, when the daily number of earthquakes was at least one order greater than its statistical average, and the seismic energy released over this month exceeded the seismic energy released over the preceding 11 months by two orders [Gusev *et al.*, 1998]. According to data of continuous GPS observations, movements of an appreciable amplitude arose a half-month before this earthquake at distances of up to a few hundred kilometers (a strain precursor); these movements were consistent with a slow M = 7.7 earthquake of the double dipole type. Also observed were distinct coseismic movement jumps at the time moment of the earthquake and intense postseismic deformations lasting for at least half a month. The overall displacement resulting from the Kronotski earthquake yielded a total seismic moment corresponding to M_w = 8.0 [Gordeev *et al.*, 2001].

Before this earthquake, weak anomalies in the ETF variations recorded at the VP station were discovered by applying a complex of multidimensional series processing algorithms to the electrotelluric observations. The inferred statistical anomalies reflected an increase in the level of asynchronous noise components in telluric potential variations recorded on individual lines [Kopylova *et al.*, 2001].

In the period from 1998 through 2001, three earthquakes with amplitudes of 6.3–6.9 occurred in Avachinskii Bay at a distance of 140–150 km from the VP station; these were the earthquakes of June 1, 1998 (M_{max} = 6.3; no. 2); March 8, 1999 (M_{max} = 6.9; no. 3); and October 8, 2001 (M_{max} = 6.6; no. 4). Numerous aftershocks followed these earthquakes.

Figure 1b plots strain values [Dobrovolskii, 1991] at various nucleation stages of $K \ge 9.0$ earthquakes with hypocentral depths $H \le 100$ km within 360 km from the VP station. This plot characterizes the influence of the nucleation processes in the VP station area. The theoretical strains at the nucleation stages of the four strong earthquakes, which occurred in the observation period (nos. 1–4 in the table), are similar and amount to a few units of $\times 10^{-7}$. The strain values in the area of the VP station are one and more orders smaller for the majority of earthquakes that occurred in this period. Strain values comparable to those estimated for earthquake nos. 1–4 were only obtained for the earthquakes of June 3, 2000 (M = 4.9); August 27, 2000 (M = 4.8); and December 20, 2000 (M = 5.6). These higher estimates are due to relatively small epicentral distances of the events from the VP station. This strain analysis of the relative influence of earthquakes in the area of the VP station suggests that the nucleation of the tabulated earthquakes gave rise to ETF variations that involved a larger area and were

more pronounced compared to the effects of other, weaker seismic events.

Weak local seismicity. The VP station is located in an area of recent tectonic movements associated with the development of the Paratunka and Karymshin grabens. The active Gorelyi and Mutnovskii volcanoes are a few tens of kilometers from the station. Weak seismicity is evidence for orogenic, volcano-tectonic, and possibly hydrothermal processes in the area. Eleven weak (K = 5.1–6.9) earthquakes occurred at hypocentral depths of 0–20 km (Fig. 1c) within 35 km from the VP station in 1996–2001. These events were distributed irregularly in time. Local seismicity was enhanced in the period from July 1997 to February 1998, when eight of the eleven earthquakes occurred. All these earthquakes had epicenters in the southern part of the Paratunka graben at distances of 26–30 km south-southwest of the VP station.

PROCESSING RESULTS

Algorithm of data processing. Let q time series $V^{(k)}(t)$, $t = 1, \ldots, N$; $k = 1, \ldots, q$; $q > 2$) represent synchronous records of ETF variations obtained from individual measuring lines. Since lower frequencies make the major contribution to recorded ETF series (Fig. 2), the initial series are transformed into series of increments. In analyzing the latter, we retain the notation of the initial series.

We introduce a *moving time window of adaptation* of r samples in width and normalize the time series to a homogeneous range of values, which is indispensable for a joint analysis of heterogeneous series of different scales:

$$U^{(k)}(t) := V^{(k)}(t)/(V^{(k)}_{\max}(1, r) - V^{(k)}_{\min}(1, r)) \quad \text{for } 1 \le t \le (r+1); \tag{1a}$$

$$U^{(k)}(s+r) := V^{(k)}(s+r)/(V^{(k)}_{\max}(s, r) - V^{(k)}_{\min}(s, r)) \quad \text{for } s > 1; \tag{1b}$$

$$V^{(k)}_{\min}(s, r) = \min_{s \le t \le s+r} V^{(k)}(t), \quad V^{(k)}_{\max}(s, r) = \max_{s \le t \le s+r} V^{(k)}(t). \tag{1c}$$

Operations (1) normalize each time series to a unit peak-to-valley value (formula (1a)) in the first adaptation window; in the subsequent windows, shifted by one sample to the right, only the rightmost sample $s + r$ is normalized, while the results of the preceding normalization remain the same (formula (1b)). In this way, variations of the initial time series are adapted to a general scale solely to the left of the current point in the window r samples wide. This approach of the *left-oriented adaptation window* is applied everywhere below, because it aims at the identification of precursory phenomena, with the "backward" influence of postseismic effects being eliminated.

In this study, we used an adaptation window 365 samples (1 year) wide, which appears to be natural for the low-frequency ETF range. Figure 3 presents the time series of telluric potential differences from lines 1 (Fig. 3a), 3 (Fig. 3b), and 4 (Fig. 3c) after the application of the preliminary operations (1) to the respective initial series. Similar to the latter (Fig. 2), the series shown in the figure retain the seasonal effect of higher variation amplitudes in spring, summer, and autumn, when the daily average temperatures are stably positive.

Orthogonal multiple-resolution analysis of a signal $x(t)$ is determined by the formula [Daubechies, 1992; Mallat, 1998]

$$x(t) = \sum_{j=-\infty}^{+\infty} x^{(\alpha)}(t),$$

$$x^{(\alpha)}(t) = \sum_{j=-\infty}^{+\infty} c^{(\alpha)}(\tau_j^{(\alpha)})\psi^{(\alpha)}(t - \tau_j^{(\alpha)}), \tag{2}$$

$$\tau_j^{(\alpha)} = j \cdot 2^{\alpha}.$$

Here, α is the number of the *detail level*;

$$c^{(\alpha)}(\tau_j^{(\alpha)}) = \int_{-\infty}^{+\infty} x(t)\psi^{(\alpha)}(t - \tau_j^{(\alpha)})dt$$

are the wavelet coefficients at the αth detail level that correspond to the time moment $\tau_j^{(\alpha)}$; and $\psi^{(\alpha)}(t)$ are basis functions of the αth level obtained by stretching and translation of the main wavelet function $\Psi(t)$,

$$\psi^{(\alpha)}(t) = (\sqrt{2})^{-\alpha}\Psi(2^{-\alpha}t), \quad \psi^{(\alpha)}(t - \tau_j^{(\alpha)}) = (\sqrt{2})^{-\alpha}\Psi(2^{-\alpha}t - j). \tag{3}$$

The function $\Psi(t)$ is constructed in such a way that it is finite and has the unit norm in $L_2(-\infty, +\infty)$. Then, the infinite set of functions $\{\psi^{(\alpha)}(t - \tau_j^{(\alpha)})\}$ that are copies of the main function shifted to the points $\tau_j^{(\alpha)}$ and stretched by 2^{α} times should form an orthonormal basis in $L_2(-\infty, +\infty)$. For example, if

$$\Psi(t) = -1 \text{ for } t \in \left(0, \frac{1}{2}\right], \quad +1 \text{ for } t \in \left(\frac{1}{2}, 1\right], \text{ and 0 for other values of } t, \tag{4}$$

formula (2) yields the expansion of the signal $x(t)$ in Haar wavelets. The most popular family of orthogonal wavelet functions consists of the Daubechies functions

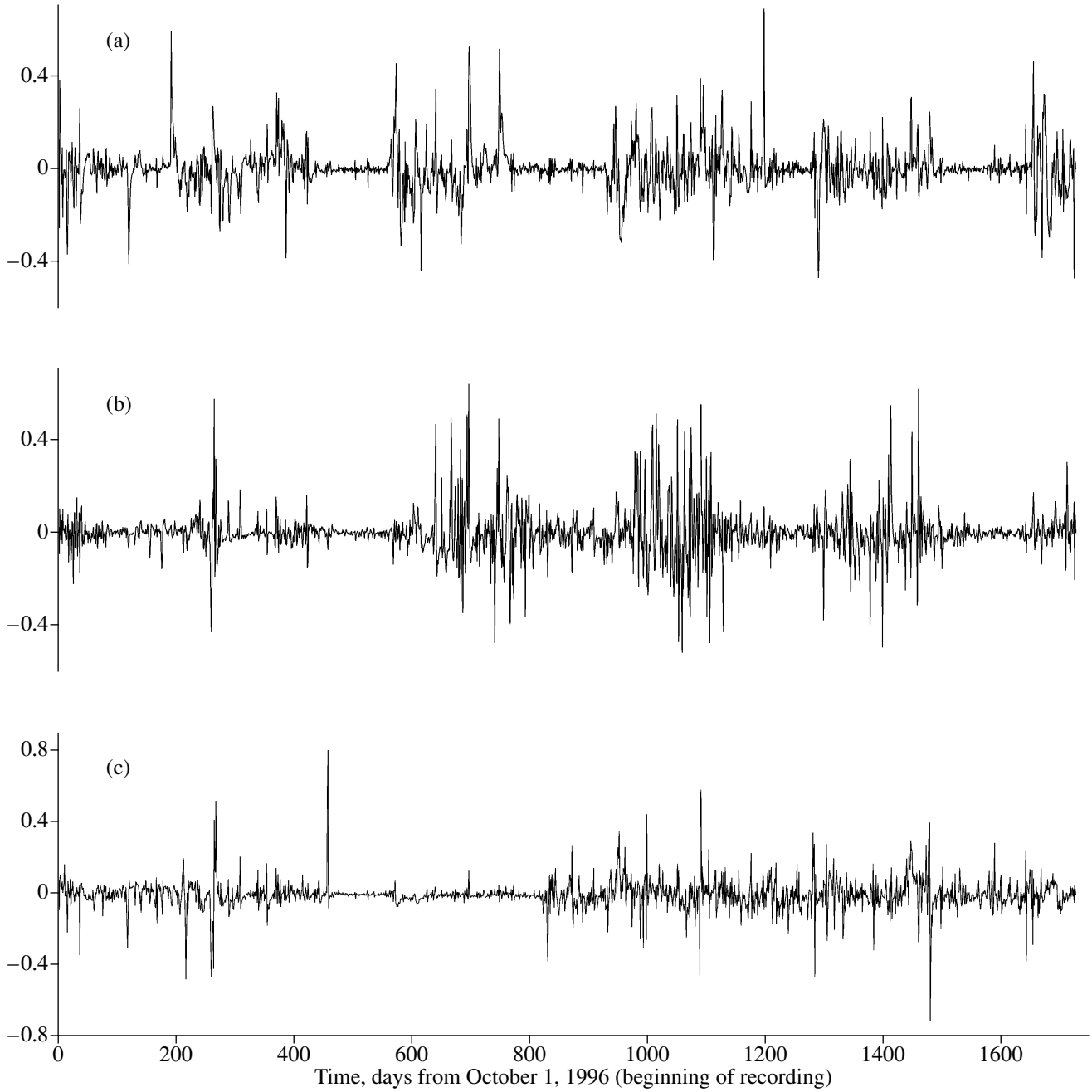

Fig. 3. Initial data after conversion to increments and left-oriented scaling in a moving time window 365 samples (days) wide: (a–c) measuring lines (a) 1, (b) 3, and (c) 4.

$\Psi(t) = D_{2p}(t)$ of order $2p$, which possess the following properties [Daubechies, 1988, 1992; Chui, 1992]:

$$D_{2p}(t) = 0 \text{ outside } [-p + 1, p],$$
$$\int_{-\infty}^{+\infty} t^k D_{2p}(t)dt = 0 \text{ for } k = 0, 1, \ldots, (p-1). \quad (5)$$

Note that the Haar wavelet (4) is a Daubechies wavelet of 2nd order ($p = 1$). The detail level can be roughly associated with the period of characteristic variations of the signal, and the number of such periods in the orthogonal wavelet analysis is significantly smaller than in the Fourier analysis. Each detail level can be brought into correspondence with a certain frequency band. The central frequency of this band has a period (measured in units of the discretization interval) equal to 2^α, where $\alpha = 1, 2, \ldots$, is the detail level number. Thus, each wavelet coefficient is characterized by two indexes: the first is the detail number α, and the second is the time index $\tau_j^{(\alpha)}$, the midpoint of the support interval of the basis function $\psi^{(\alpha)}(t)$.

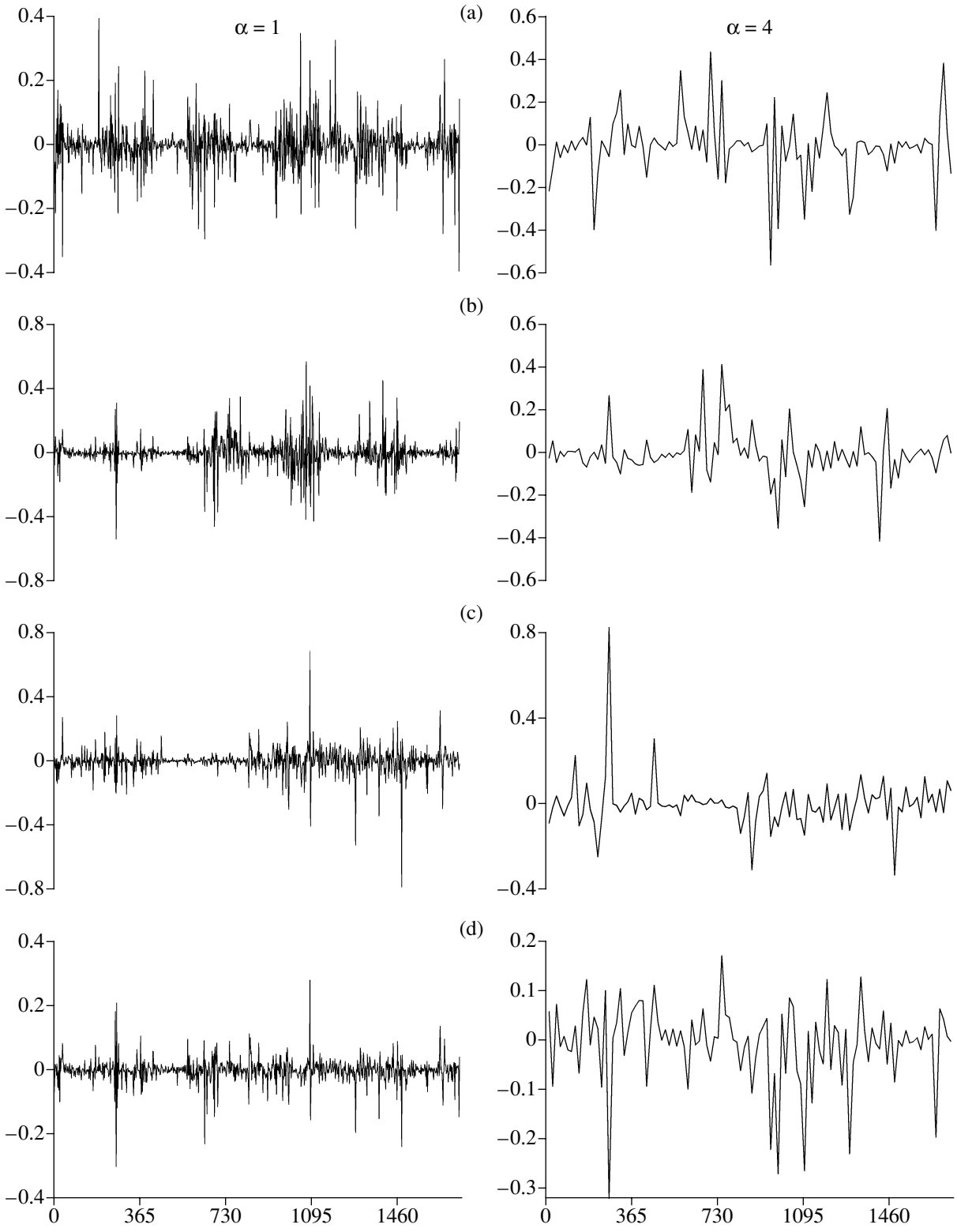

Fig. 4. Wavelet coefficient at the 1st (on the left) and 2nd (on the right) detail levels α for initial data after applying the procedures of transition to increments and scaling: (a–c) measuring lines (a) 1, (b) 3, and (c) 4; (d) results of robust aggregation of signals from the three measuring lines. Haar wavelets, a window 365 samples (days) wide, and $L_{\min} = 10$ were used. The time in days from October 1, 1996 (beginning of recording) is laid off on the horizontal axis.

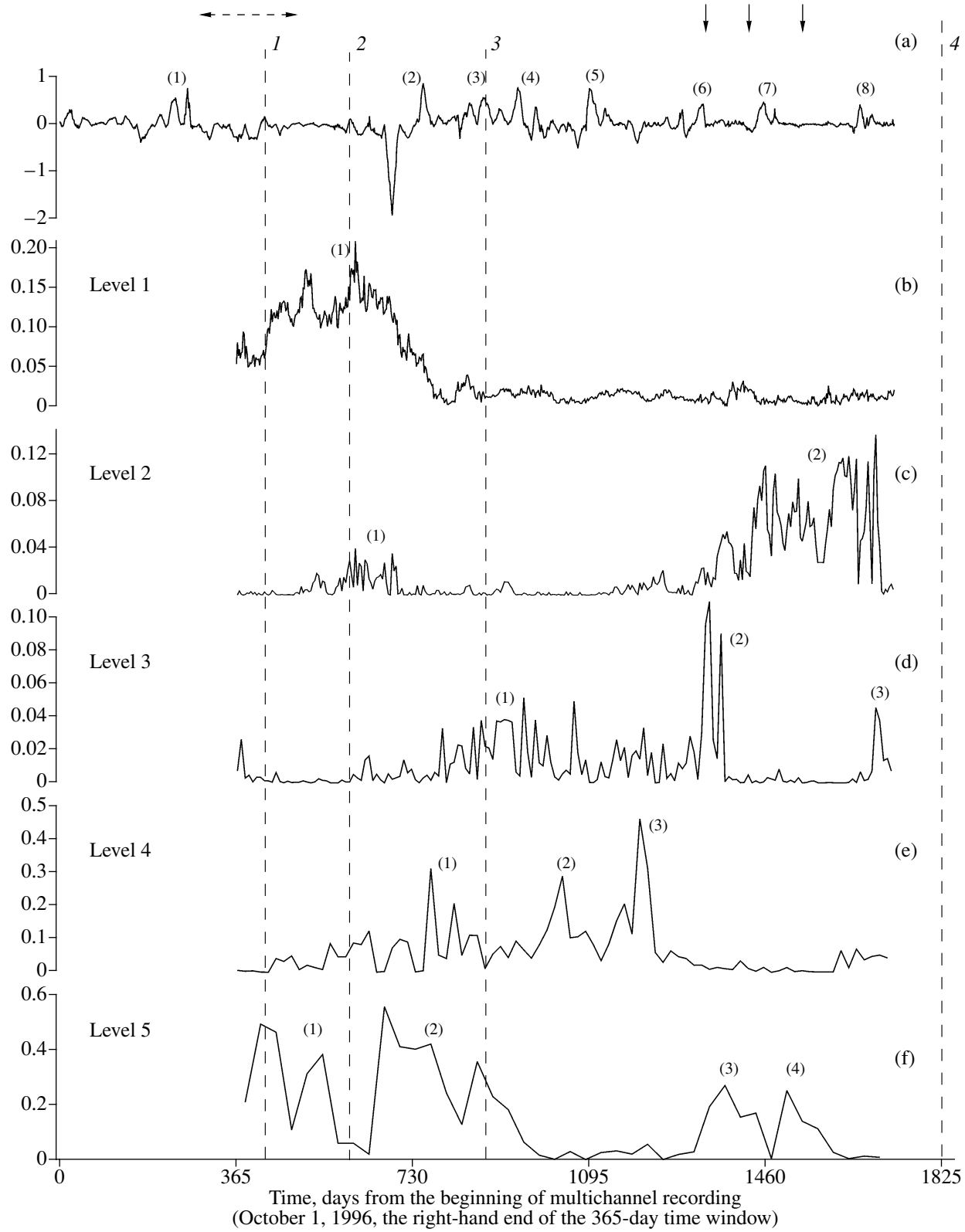

Fig. 5. (a) Robust wavelet-aggregated signal (AS) and (b–f) evolution of the product of canonical correlations $\kappa(\tau, \alpha)$ between components at various detail levels. The vertical broken lines indicate time moments of strong earthquakes (their numbers are the same as in Fig. 1 and the table). The vertical arrows indicate earthquakes of 2000 (see the table). The horizontal broken line is the activation period of local seismicity. The numbers with a parenthesis denote intervals of higher values of the AS and $\kappa(\tau, \alpha)$ (see explanations in the text).

The higher the order of wavelet functions, the smoother they are and, therefore, the more suitable for analysis of smooth functions. The Haar wavelet is beneficial to the extraction of sharp, steplike components from the signal. With larger detail level indexes α, the wavelet coefficients $c^{(\alpha)}(\tau_j^{(\alpha)})$ characterize larger-scale (low-frequency) variations of the signal $x(t)$ in the vicinity of the points $\tau_j^{(\alpha)}$ specified on a coarser mesh. Taking into account the shape of the plotted data (Fig. 3) and their undoubtedly jumplike behavior, we chose Haar wavelets (4) as the most suitable for analysis.

As an example, Figs. 4a–4c present the wavelet coefficient plots of the ETF time series at the first and fourth detail levels after applying preliminary transformations (1). Note that the wavelet coefficients at the fourth and fifth detail levels (approximately corresponding to variation periods of 16 and 32 days) have specific features distinguishing their behavior from wavelet coefficients at the first to third detail levels (approximate variation periods of 2–8 days). Variations of the latter are, on the whole, similar to the behavior of the initial normalized series of recorded ETF data (Fig. 3) and are dominated by seasonal components. The measured potential variations having periods longer than 8 days evidently reflect ETF variations unrelated to seasonal effects.

In processing the wavelet coefficients of the initial time series (after application of the normalization operations (1)), they are brought into correspondence with the so-called canonical wavelet coefficients, obtained from the canonical correlation analysis of covariance matrices of wavelet coefficients at each detail level. Canonical wavelet coefficients of a given series k are calculated as linear combinations of wavelet coefficients of all other time series, and the parameters of these combinations are determined from the condition of the maximum modulus of the correlation coefficient $\nu_k(\tau, \alpha)$ between the wavelet coefficients of the series under consideration k and a linear combination of wavelet coefficients of all other series. This value depends on the detail level index α and the parameter τ of the moving time window. Since sample estimates of covariance matrices are considered, we introduce such a parameter of the algorithm as the representativeness threshold $L_{\min}$. The parameter $L_{\min}$ defines the smallest admissible number of wavelet coefficients that can be used for sample estimation of the covariance matrix at a given detail level within the moving adaptation time window of a given width. As a result, the joint analysis of time series is only applicable to a certain number of first detail levels, depending on the window width and the representativeness threshold. We used the value $L_{\min} = 10$. Given the adaptation window width $r = 365$, this value of $L_{\min}$ enables the analysis of five detail levels, approximately corresponding to ETF variation periods of 2–32 days.

In this work, we measured the collectiveness of variations of the initial ETF signals recorded on separate lines by the value $\kappa(\tau, \alpha)$, which is the product of the moduli of all canonical intercomponent correlation coefficients $\nu_k(\tau, \alpha)$. The value $\kappa(\tau, \alpha)$ is estimated within a moving adaptation window r samples wide, with τ being the number of the rightmost sample in the window, and ranges from zero to unity. Thus, the closer the value of $\kappa(\tau, \alpha)$ to unity, the more collective the variations of initial data within the r-sample time window adjacent to the point τ on its left side.

Moreover, for each detail level α in the moving time window, we calculated the first principal components of the canonical wavelet coefficients of all analyzed time series, the so-called aggregated wavelet coefficients. The inverse wavelet transformation of the aggregated wavelet coefficients provides an aggregated signal (AS). Plots of the aggregated signal and aggregated wavelet coefficients at each detail level can also serve as indicators of collective signals in variations of the initial series on various time scales. Figure 4d presents the plots of aggregated wavelet coefficients at the first and fourth detail levels for the three time series analyzed.

We should note that all operations described above qualitatively were implemented in a robust variant. A detailed description of the computational technology can be found in [Lyubushin, 2002].

Figure 5 presents plots illustrating the results of the aggregation procedure applied to the initial recorded ETF data from three measuring lines of the VP station with the use of the Haar wavelets at $r = 365$ and $L_{\min} = 10$. Plots of the aggregated signal and collectivity measures of variations $\kappa(\tau, \alpha)$ at $\alpha = 1, \ldots, 5$ are shown successively from top to bottom.

DISCUSSION OF RESULTS OF THE ANALYSIS

Two effects in the variations of the aggregated signal and $\kappa(\tau, \alpha)$ as a measure of the collective ETF behavior at various detail levels are noteworthy in Fig. 5. The first effect is the presence of a few weakly pronounced intervals of higher values of the wavelet coherence measure (Fig. 5a), indicating enhancement of the collective ETF variations specified by the Haar wavelet (4). The second effect is noticeable as asynchronous peaks of the collective ETF behavior measure $\kappa(\tau, \alpha)$ at various α and a tendency of their migration toward shorter periods (Figs. 5b–5f).

AS variation in relation to seismicity. Eight intervals of higher AS values with amplitudes $\geq|0.4|$ are recognizable in Fig. 5a. These intervals, indicated by numbers with a parenthesis, are compared with occurrence

times of strong earthquakes, local seismicity activation, and hydrometeorological conditions:

(1) June–July 1997	$\Delta T \approx 2$ months	Activation of local seismicity
(2) August–September 1998	$\Delta T \approx 3$ months	Precipitation
(3) February 1999	$\Delta T \approx 1$ months	Earthquake of March 8, 1999 (no. 3)
(4) May–June 1999	$\Delta T \approx 1$ months	Snow melting
(5) September–early October 1999	$\Delta T \approx 1.5$ months	Precipitation
(6) May 2000	$\Delta T \approx 1$ months	Snow melting
(7) September 2000	$\Delta T \approx 1$ months	?
(8) April 2000	$\Delta T \approx 1$ months	Snow melting

The above analysis shows that an increase in the collective behavior of variations in interval (3) of February 1999 could be due to the nucleation of the strong earthquake of March 8, 1999 (no. 3). A maximum strain estimate was obtained for the nucleation stage of this earthquake in the area of the VP station (Fig. 1b; table). The AS amplitude increase in June–July 1997 (interval (1)) preceded an activation of local seismicity and could be caused by the increase in the collective behavior of the ETF variations due to tectonic and related fluid-dynamic processes in the southern part of the Paratunka graben. Intervals (2), (4)–(6), and (8) coincide with either periods of spring melting of snow or periods of heavy precipitation. Thus, only in one of eight cases of higher values of the AS amplitude can such a signal of enhancement in the collective ETF behavior be related to the nucleation of a strong earthquake.

The overall duration of intervals of higher AS amplitudes amounts to about 12.5 months, i.e., 22% of the entire observation period 56 months long. Taking into account that an AS anomaly was observed before only one of the three strongest earthquakes that occurred in the ETF observation period, the probability of successful prediction amounts to 1/3 = 0.33. Then, the efficiency of strong earthquake prediction based on such an indicator as the increase in the AS amplitude is 0.33/0.22 = 1.5, the probability of a causative relation between a precursory AS anomaly and a strong earthquake being equal to 0.125 [Gusev, 1974]. This is evidence for a rather weak statistical relationship between anomalous low-frequency increases in the AS amplitude and strong earthquakes and indicates the complexity and multifactor origins of the formation of collective ETF variations in the VP station area. Moreover, the contribution of nucleation processes of strong earthquakes to raising the overall collectivity of ETF variations is far from being predominant.

Structure and migration of the collectivity measure of ETF variations. We address the time intervals and periodicity of increases in the values $\kappa(\tau, \alpha)$ at various levels α (Figs. 5b–5f):

α	Time interval	Length	Earthquakes
Level 1	(1) October 1997–September 1998	$\Delta T_2 = 12$ months	nos. 1 and 2
Level 2	(1) March–August 1998	$\Delta T_2 = 6$ months	no. 2
	(2) July 2000–May 2001	$\Delta T_2 = 9$ months	2 events of 2000
Level 3	(1) December 1998–February 2000	$\Delta T_2 = 14$ months	no. 3
	(2) May–June 2000	$\Delta T_1 = 2$ months	1 event of 2000
	(3) May 2001	$\Delta T_1 = 1$ month	
Level 4	(1) November 1998–February 1999	$\Delta T_2 = 4$ months	no. 3
	(2) July–August 1999	$\Delta T_1 = 2$ months	
	(3) December 1999–February 2000	$\Delta T_1 = 3$ months	
Level 5	(1) November 1997–April 1998	$\Delta T_2 = 5$ months	nos. 1 and 2
	(2) July 1998–March 1999	$\Delta T_2 = 9$ months	no. 3
	(3) June–July 2000	$\Delta T_1 = 2$ months	2 events of 2000
	(4) November 2000	$\Delta T_1 = 1$ month	1 event of 2000

The lengths (ΔT) of intervals of higher values of $\kappa(\tau, \alpha)$ vary from 1 to 14 months and are divided into two groups. The first group includes intervals ΔT_1 1–3 months long (six intervals), and the second includes intervals ΔT_2 4–14 months long (seven intervals). Most intervals of the first group (5 of 6) belong to spring, summer, or autumn seasons and can be caused by seasonal factors affecting the ETF variations due to a higher water content and activation of electrokinetic, ionic-diffusion, and other processes, mainly in the aeration zone of the observation area. However, some of these intervals (e.g., 2) of level 3 and (3) and (4) of level (5) preceded earthquakes of 2000 (see the table) characterized by higher strain estimates in the VP station area.

Higher values of $\kappa(\tau, \alpha)$ in intervals of the second group (ΔT_2) are unrelated to seasonal or hydrometeorological factors. They associate, to an extent, with higher seismic activity periods and strong earthquake occurrence times. Six of the seven intervals of the second group either preceded or included time moments of strong earthquakes (they are boldfaced in Figs. 5b–5f). This indicates that enhanced collective behavior of ETF variations at various detail levels can reflect both nucleation processes of strong earthquakes and their postseismic effects.

The variations in $\kappa(\tau, \alpha)$ shown in Figs. 5b–5f exhibit successive migration of collectivity measure peaks from lower- to higher-frequency detail levels. Note that this phenomenon (an increase in the frequency of collective variations) has long been known in the literature devoted to critical phenomena and has been utilized in analyses of both geophysical and financial data, albeit beyond the scope of multidimensional data analysis [Johansen *et al.*, 1996; Sornette *et al.*, 1996].

A particular pronounced episode of such a migration (I) is observed at detail levels 5–2 if the group of intervals (1) and (2) is accepted as the starting moment of the migration. These increases in the collective behavior are replaced at level 4 by the joint appearance of higher $\kappa(\tau, \alpha)$ intervals (1)–(3). Furthermore, intervals (1) and (2) appearing at level 3 change for the long interval (2) at level 2. The duration of such migration features appearing at certain levels as long intervals of higher values of $\kappa(\tau, \alpha)$ is on the order of one or two years. The distinct $\kappa(\tau, 1)$ maximum of interval (1) from late 1997 through 1998 can either continue the preceding migration cycle or be unrelated to this cycle if migration manifestations are confined to the range of relatively short periods of ETF variations. A less pronounced migration cycle (II) of the collectivity measure $\kappa(\tau, \alpha)$ is observed at levels 5–3, starting from intervals (3) and (4) at level 5.

The most pronounced migration cycle (I) could be related to the strongest Kronotski earthquake and the related geodynamic processes in the junction zone of the Pacific and Sea of Okhotsk plates. The regional scale of these processes is evident, for example, from changes in the velocities of movement of Kamchatka GPS stations before and after this earthquake [Gordeev *et al.*, 2001]. The less pronounced migration cycle (II) preceded the strong earthquake of October 8, 2001, which occurred after the relatively quiescent period 2.5 years long, and can be related to the nucleation processes of this event.

The inferred structural features of the variations in AS and $\kappa(\tau, \alpha)$ (as a collectivity measure of ETF variations in the time and frequency domains) appear to indicate a process responsible for temporal variations in the ETF sensitivity to seismotectonic processes. Such a process in the VP station area is most likely associated with the development of the hydrogeological structure and hydrothermal system of the Paratunka and Karymshin grabens under the concurrent action of tectonic, volcanic, and exogenous factors resulting in deformation of the geological medium in the observation area. Elastic and inelastic deformation of hydrogeological structures differing in scale gives rise to variations in the fluid-dynamic regime and activates hydrogeodynamic and gaseous-hydrogeochemical processes leading to general changes in the physicochemical conditions in the VP station area. Development of relatively slow seismo- and volcanotectonic processes accompanied by deformation of a fluid-saturated heterogeneous multiphase medium can be associated with mechanoelectrical conversion phenomena, with a leading role of electrokinetic and ionic-diffusion processes [*Electromagnetic Precursors* …, 1982; Svetov *et al.*, 1997].

CONCLUSION

A well-pronounced amplitude signal in the initial temporal ETF series is the seasonal component, observable as low-frequency variations in daily average differences of telluric potentials on individual lines (Fig. 2) and an increase in the variance of the normalized time series in spring, summer, and autumn time (Fig. 3). The seasonal effects are most distinct on lines 1 and 3 and, to a lesser extent, on line 4. This is likely related to local structural features in the areas of the measuring lines, which in turn affect local fluid-dynamic patterns in rocks of the aeration zone and control the mosaic structure of background ETF variations. The seasonal effects in the behavior of wavelet coefficients and their aggregated time series (Fig. 4) are much weaker or nearly unrecognizable (at higher detail levels). This indicates that the algorithm of robust wavelet aggregation, when applied to multivariate series of electrotelluric observations, weakens the effect of the most intense low-frequency interference and effectively identifies specific signals of an increase in the collective behavior of ETF variations at various detail levels, specified by the Haar wavelet.

Asynchronous periods of an increase in $\kappa(\tau, \alpha)$ identified in temporal ETF series of recorded data at various detail levels might reflect contributions of different volumes of the medium and, possibly, different mechanoelectrical processes to the collective ETF behavior, depending on the direction of measuring lines. The successive migration of collectivity measure peaks toward higher-frequency levels suggests that this phenomenon is controlled, to an extent, by an energy-dissipating process spatially evolving from larger to smaller scales. The Kronotski earthquake of December 5, 1997, and related large-scale geodynamic and seismic processes at the boundary between the Pacific and Sea of Okhotsk plates could serve as a triggering factor of such an energy impulse. The migration of stronger ETF synchronization periods toward higher frequencies could be a specific signature of these processes in the

ETF variations in the area of recent volcanism and hydrothermal activity.

A certain coincidence in time of periods of higher collectivity of low-frequency ETF variations with the occurrence of strong and moderate earthquakes is evidence for a link between the seismotectonic process and the electrotelluric field in Kamchatka. However, the problem of the concrete mechanism and stability of the relationship of the inferred ETF features with individual earthquakes and, in particular, with the nucleation of strong earthquakes is still unclear, which precludes the development of a prognostic algorithm. Presently, this is primarily due to the impossibility of specifying a criterion (or criteria) for the discrimination between ETF signals of strong earthquake nucleation and signals produced by other geodynamic factors (in particular, local tectonic, volcano-tectonic, and other processes accompanied by rock deformations). Apparently, such criteria are difficult to elaborate because the majority of "desired" low-frequency ETF signals are likely due to variations in the fluid-dynamic regime that, irrespective of the origin of the deformations, can generate signatures of a similar type, controlled by geological and hydrogeological conditions in the observation area.

Data of electrotelluric observations can be used for earthquake prediction more effectively if they are analyzed in conjunction with strainmetering, hydrogeodynamic, hydrogeochemical, and other data. Such a complex of sufficiently detailed, continuous, and long-term observations can provide deeper insights into the origin and sources of anomalous signals in the electrotelluric field.

REFERENCES

1. *Active Volcanoes in Kamchatka* (Moscow, Nauka, 1991), Vol. 2 [in Russian].
2. S. T. Balesta, G. N. Kopylova, E. R. Latypov, and Yu. D. Kuz'min, Vulkanol. Seismol., Nos. 4–5, 90 (1999).
3. I. Daubechies, *Ten Lectures on Wavelets (CBMS-NSF Series in Applied Mathematics, No. 61)* (Philadelphia, SIAM, 1992).
4. A. V. Deshcherevsky and A. Ya. Sidorin, Fiz. Zemli, No. 1, 87 (2000) [Izvestiya, Phys. Solid Earth **36**, 78 (2000)].
5. I. P. Dobrovolskii, *Mechanics of the Tectonic Earthquake Nucleation* (Moscow, Nauka, 1991).
6. *Electromagnetic Precursors of Earthquakes* (Moscow, Nauka, 1982) [in Russian].
7. M. B. Gokhberg, V. A. Morgunov, and O. A. Pokhotelov, *Seismoelectromagnetic Phenomena* (Moscow, Nauka, 1988) [in Russian].
8. E. I. Gordeev, A. A. Gusev, V. E. Levin, *et al.*, Geophys. J. Int., **147**(1), 189 (2001).
9. A. A. Gusev, in *Seismicity, Seismic Prediction, Upper Mantle Properties, and Implications for the Kamchatka Volcanism* (Novosibirsk, Nauka, 1974), pp. 109–119.
10. A. Johansen, D. Sornette, H. Wakita, *et al.*, J. Phys. (Paris), No. 6, 1391 (1996).
11. *Kamchatka: Kurile and Komandorskie Islands. The Relief Development History in Siberia and the Far East* (Moscow, Nauka, 1974) [in Russian].
12. G. N. Kopylova, A. A. Lyubushin, Jr., and L. N. Taranova, in *Problems of Geodynamics and Earthquake Prediction*, Ed. by F.G. Korchagin (Khabarovsk, ITiG DVO RAN, 2001), pp. 225–245 [in Russian].
13. A. A. Lyubushin, Jr., Fiz. Zemli, No. 3, 69 (1998) [Izvestiya, Phys. Solid Earth **34**, 238 (1998)].
14. A. A. Lyubushin, Jr., Earthquake Res. China **13** (1), 33 (1999).
15. A. A. Lyubushin, Jr., Fiz. Zemli, No. 3, 20 (2000) [Izvestiya, Phys. Solid Earth **36**, 204 (2000).
16. A. A. Lyubushin, Jr., Fiz. Zemli, No. 6, 41 (2001) [Izvestiya, Phys. Solid Earth **37**, 474 (2001).
17. A. A. Lyubushin, Jr., Fiz. Zemli, No. 9 (2002) [Izvestiya, Phys. Solid Earth **38**, 745 (2002)].
18. S. Mallat, *A Wavelet Tour of Signal Processing* (San Diego, Academic, 1998).
19. Yu. Manukhin and L. A. Vorozheikina, in *Hydrothermal Systems and Thermal Fields in Kamchatka*, Ed. by V. M. Sugrobov (Vladivostok: DVNTs AN SSSR, 1976), pp. 143–178 [in Russian].
20. Yu. F. Moroz, V.F. Bakhtiarov, V.F. Voropaev, *et al.*, Vulkanol. Seismol., Nos. 4–5, 139 (1995).
21. G. A. Sobolev, *Fundamentals of Earthquake Prediction* (Moscow, Nauka, 1993) [in Russian].
22. G. A. Sobolev and V. N. Morozov, in *Seismicity, Seismic Prediction, Upper Mantle Properties, and Implications for the Kamchatka Volcanism* (Novosibirsk, Nauka, 1974), pp. 14–151 [in Russian].
23. D. Sornette, A. Johansen, and J.-Ph. Bouchaud, J. Phys. (Paris) **6**, 167 (1996).
24. B. S. Svetov, S. D. Karinskii, S. D. Kuksa, and V. I. Odintsov, Fiz. Zemli, No. 5, 36 (1997).
25. S. Uyeda, in *A Critical Review of VAN* (World Scientific Publishing Co. Pte. Ltd., 1996), pp. 1–26.